Chem

CellPress

Controlled Synthesis of Pt^{II} and Pd^{II} Supramolecular Copolymers with Sequential Multi-blocks and Amplified Phosphorescence

Qingyun Wan[1], Wai-Pong To[1], Xiaoyong Chang[2], and Chi-Ming Che[1,3,4 *]

[1] Department of Chemistry and State Key Laboratory of Synthetic Chemistry, The University of Hong Kong, Pokfulam Road, Hong Kong, China
[2] Department of Chemistry, Southern University of Science and Technology of China, Shenzhen, Guangdong 518055, China
[3] HKU Shenzhen Institute of Research & Innovation, Shenzhen 518057, China
[4] Lead Contact
* Correspondence: cmche@hku.hk

SUMMARY

Supramolecular copolymers constitute a fundamental new class of functional materials attracting burgeoning interest, but examples that display phosphorescence and long-lived excited states are rare. Herein, we describe the synthesis of sequential phosphorescent multi-block supramolecular copolymers in one and multiple dimensions using pincer Pt^{II} and Pd^{II} complexes as building blocks by manipulating out-of-equilibrium self-assemblies via the living supramolecular polymerization approach. Doping a small amount of Pt^{II} complexes (2 mol%) into the Pd^{II} assemblies significantly boosted the emission efficiency and radiative decay rate constant (Φ_{em} = 3.7%, $k_r = 1.8\times10^4$ s^{-1} in Pd^{II} assemblies; Φ_{em} = 76.2%, $k_r = 58.6\times10^4$ s^{-1} in Pt^{II}-Pd^{II} co-assemblies), which is ascribed to an external heavy-atom spin-orbital coupling effect arising from the doped Pt^{II} complex with a delocalized ^{3}[dσ*→π*] excited state. The findings on Pt^{II} and Pd^{II} supramolecular copolymers with controlled sequences and greatly enhanced phosphorescence efficiencies open the door to new photofunctional/responsive luminescent metal-organic supramolecular materials.

Key Words: living supramolecular polymerization, multi-block supramolecular copolymer, platinum and palladium, external heavy-atom effect, phosphorescence

INTRODUCTION:

Supramolecular polymers, which are aggregated small molecules linked by non-covalent forces, display highly dynamic and flexible monomer-to-polymer transitions.[1-7] In polymer science, living polymerization is used to prepare multi-functional copolymers under control. Recently, living supramolecular polymerization has been conceptualized and utilized to make intriguing supramolecular polymers.[8-16] Synthesis of multi-block supramolecular copolymers with sophisticated structural complexity could therefore be achieved.[17] To synthesize supramolecular copolymers with precise control, an in-depth understanding of the corresponding pathway complexity and delicate control of various kinetic/thermodynamic aggregates of different components are crucial; however, these challenges remain formidable. Despite possessing enormous potential in information storage, heterojunction semiconductors, gels and drug delivery in biological science,[18-23] supramolecular multi-block copolymers are scarce in the literature.[17,22,24-26] Pioneering works by Manners, Winnik, Friend and co-workers have presented the preparation of fluorescent sequential copolymers via a crystallization-driven self-assembly approach.[18,19,25,27] Pavan, Takeuchi, Sugiyasu and co-workers reported the synthesis of porphyrin-based supramolecular block copolymers consisting of different metal porphyrins.[17] Using thermodynamic and kinetic control, Meijer and Palmans,[24] Aida and Fukushima[22] and the Würthner group[28] prepared non-covalent block copolymers. However, block supramolecular copolymers exhibiting long-lived phosphorescence are very rare in the literature.[29]

Organometallic Pt^{II} and Pd^{II} complexes are well documented to exhibit closed-shell metal-metal interactions and MMLCT (metal-metal-to-ligand charge transfer, [dσ*→π*]) excited states upon aggregation,[30,31] with diverse applications in the field of optoelectronic devices,

sensing and light-harvesting materials.[31-34] Herein, we show that pincer-type Pd^{II} and Pt^{II} assemblies can be linked by non-covalent intermolecular interactions and form phosphorescent sequential supramolecular copolymers in both one and multiple dimensions. In the literature, extensive research activities have been reported to develop phosphorescent Pt^{II} complexes,[32-36] while examples of luminescent Pd^{II} complexes with decent phosphorescence efficiencies at room temperature remain relatively scarce.[37,38] Generally, Pt^{II} complexes possess high emission quantum yields and large k_r values due to their strong heavy-atom effect and large spin-orbit coupling constant.[37,38] In contrast, Pd is a less-heavy metal than Pt (spin-orbit coupling constant = 1412/4000 cm^{-1} for Pd/Pt), and the Pd^{II} $4d_{z^2}$ orbital is relatively lower in energy than the corresponding Pt^{II} $5d_{z^2}$ orbital, which hinders the involvement of metal character in the frontier molecular orbitals (MOs) and further decreases the k_r value. Therefore, Pd^{II} complexes usually display weak phosphorescence or prompt fluorescence because of less-efficient ISC (inter-system crossing) and $T_1 \rightarrow S_0$ radiative decay.[37-39] One of the strategies to improve the phosphorescence efficiency of Pd^{II} complexes is to decrease the structural distortion (suppress the non-radiative decay pathway) by using a rather rigid ligand scaffold or to deactivate metal-centred ^{3}[d-d] excited state by incorporating a strong-field C-atom donor ligand.[40-42] In this work, we found that by doping with a small amount (as low as 0.5 mol%) of Pt^{II} complexes during a kinetically controlled co-assembly process with Pd complexes,[43] external perturbation induced by heavy Pt atoms could significantly increase the k_r and emission quantum yield of Pt^{II}-Pd^{II} supramolecular copolymers. Moreover, the emission energy could be tuned by employing different Pt^{II} complexes. These observations indicate the potential of using supramolecular polymerization to design novel phosphorescent materials with high emission efficiency and tunable emission energy.

RESULTS AND DISCUSSION

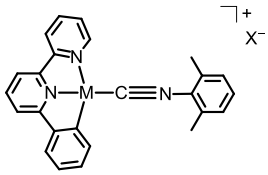

M = Pd
X = PF_6 **Pd-1-PF_6**
X = ClO_4 **Pd-1-ClO_4**
X = OTf **Pd-1-OTf**

M = Pt
X = PF_6 **Pt-1-PF_6**
X = OTf **Pt-1-OTf**

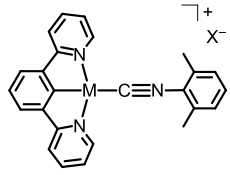

M = Pd
X = ClO_4 **Pd-2-ClO_4**
X = OTf **Pd-2-OTf**

M = Pt
X = PF_6 **Pt-2-PF_6**
X = ClO_4 **Pt-2-ClO_4**

Scheme 1. Chemical structures of the Pd^{II} and Pt^{II} complexes.

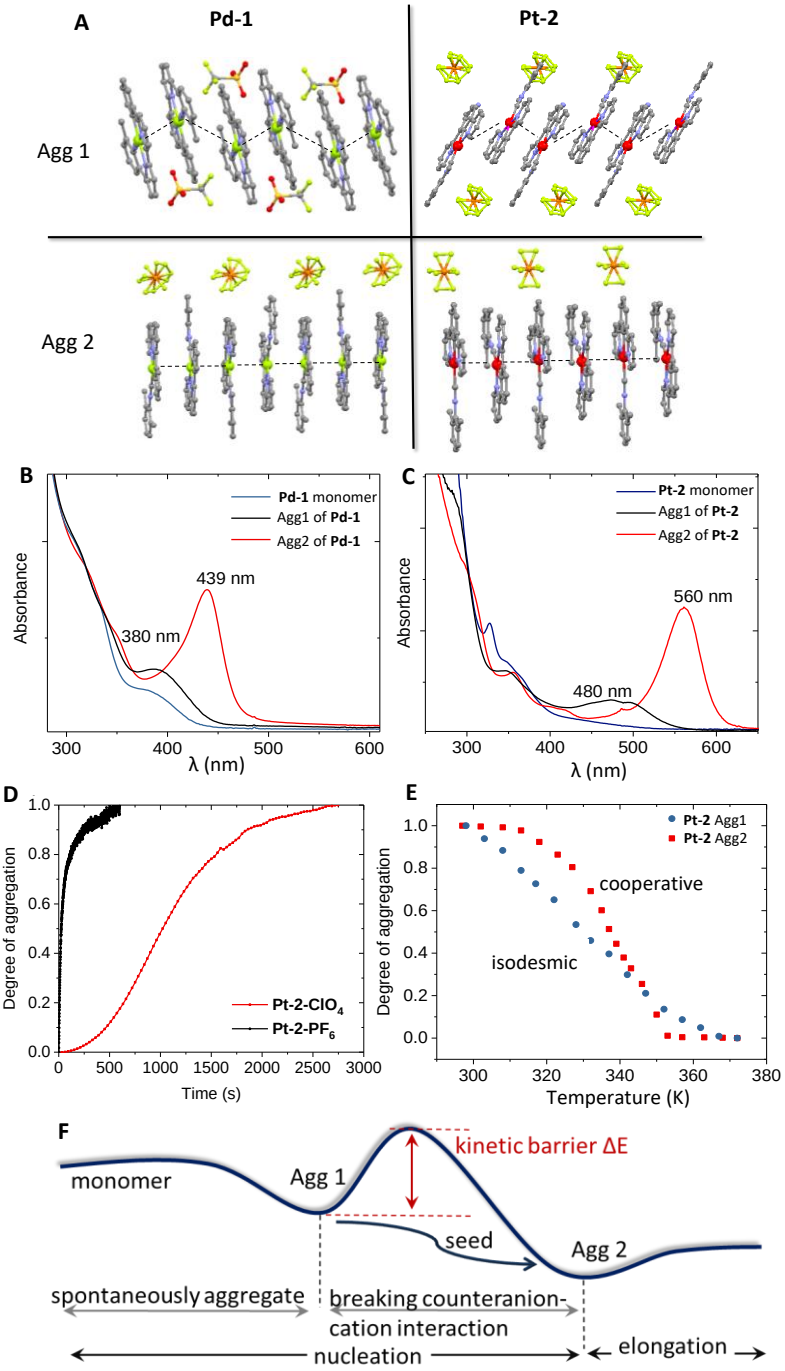

Figure 1. X-ray crystal structures, UV/Vis absorption spectra and mechanism of the supramolecular polymerization.

(A) Crystal structure of **Pd-1-PF$_6$** (bottom left) featuring an infinite 1D structure with a Pd^{II}-Pd^{II} chain; **Pd-1-OTf** (top left) featuring a cation pair structure; **Pt-2-PF$_6$** (bottom right, red crystal) featuring an infinite 1D structure with a Pt^{II}-Pt^{II} chain; **Pt-2-PF$_6$** (top right, yellow crystal) featuring a cation pair structure. Hydrogen atoms are omitted for clarity. (B) UV/Vis absorption spectra of monomers of **Pd-1-PF$_6$** in CH_3CN and Agg1 of **Pd-1-OTf** (thermodynamic aggregate state) and Agg2 of **Pd-1-PF$_6$** (thermodynamic aggregate state) in H_2O/CH_3CN (90:10 v/v) at 1×10^{-4} M. (C) UV/Vis absorption spectra of monomers of **Pt-2-PF$_6$** in CH_3CN and Agg1 of **Pt-2-ClO$_4$** (kinetic aggregate state) and Agg2 of **Pt-2-PF$_6$** (thermodynamic aggregate state) in H_2O/CH_3CN (90:10 v/v) at 1×10^{-4} M. (D) Time-dependent degree of aggregation of **Pt-2-PF$_6$** and **Pt-2-ClO$_4$** (calculated from the absorption at 560 nm in UV/Vis absorption spectra) at a concentration of 1.5×10^{-4} M (H_2O/CH_3CN, 95:5 v/v). (E) Plot of the degree of aggregation, calculated from the absorbance at 480 nm for Agg1 of **Pt-2-ClO$_4$** and at 560 nm for

Agg2 of **Pt-2-ClO$_4$** from UV/Vis absorption spectra, as a function of temperature. (F) Qualitative energy landscape of supramolecular polymerization for pincer-type Pt^{II} and Pd^{II} complexes.

Background and supramolecular polymerization pathway

In the literature, a series of cationic pincer-type Pd^{II}/Pt^{II}-isocyanide complexes were reported to possess two types of X-ray crystal structures with different intermolecular cation-cation and cation-counteranion distances,[30,44-46] providing invaluable insights into their supramolecular polymerization pathway. Of the complexes studied in this work (Scheme 1), **Pd-1**, **Pt-1** and **Pt-2-PF$_6$** were reported previously,[30,44-46] and **Pd-2-PF$_6$**, **Pd-2-ClO$_4$**, **Pt-2-ClO$_4$** are new complexes. X-ray crystal structures resolved for the Pd^{II} complexes **Pd-1-PF$_6$**/**Pd-1-OTf**[30] and the Pt^{II} complexes **Pt-1-PF$_6$**[45,46]/**Pt-2-PF$_6$**[44] show one type of discrete cation-pair structure having close contact with counteranions and another type with an infinite M-M···M (M = Pt^{II}/Pd^{II}) linear chain structure (Figure 1A). The dimer pairs and M-M···M chain-type species are termed "aggregate 1" (Agg1) and "aggregate 2" (Agg2), respectively. The aggregation of the cationic Pt^{II} or Pd^{II} complexes is induced by injecting water into their acetonitrile solutions, leading to the formation of Agg1 or Agg2. The **Pd-1** complex in the Agg1 state displays a broad absorption band at approximately 380 nm, while the **Pd-1** complex in the Agg2 form exhibits an intense absorption band at approximately 439 nm (Figure 1B).[30] For the **Pt-2** complex, the Agg1 form (yellow crystal) exhibits a broad absorption band at approximately 480 nm, while the Agg2 form (red crystal) shows an intense absorption band at approximately 560 nm (Figure 1C). The lowest-energy absorption bands of Agg1 and Agg2 were assigned to mixed ^{1}IL (intra-ligand)-^{1}MLCT (metal-to-ligand charge transfer) and ^{1}MMLCT excited states accordingly.[30] Cationic Pt^{II}/Pd^{II} complexes with PF_6^-/ClO_4^- as counteranions were found to be first trapped in a kinetic metastable aggregate state (Agg1) upon aggregation, during which a time-dependent UV/Vis spectral change indicating a transformation from the Agg1 state to the Agg2 state was observed in a time course (Figure S2).[30] In contrast, cationic Pt^{II}/Pd^{II} complexes with OTf^- as counteranions showed no time-dependent UV/Vis spectral changes and were stable in the Agg1 state for over one week.[30] The rate of supramolecular polymerization is highly dependent on the counteranion of the complex, as depicted in Figure 1D. A lag (~200 s) was observed for **Pt-2-ClO$_4$** during the self-assembly process but was absent for **Pt-2-PF$_6$**. An isodesmic model was assigned to the self-assembly of Agg1 species of complex **Pt-2-ClO$_4$**, and a cooperative nucleation-elongation model was assigned to that of Agg2 species by analysing temperature-dependent UV/Vis absorption spectra (Figure 1E). The temperature-dependent UV/Vis absorption spectral changes of complex **Pd-1-PF$_6$**/**Pt-2-PF$_6$** in the Agg2 state showed obvious differences upon heating and cooling (Figures S3-S4), indicative of distinct hysteresis effects and the existence of a high kinetic barrier during the self-assembly pathway.[47] The supramolecular polymerization pathway is depicted in Figure 1F based on these structural and spectroscopic data.[3,30,48,49] As shown in Figure 1F, upon aggregation, the monomers are first trapped into the kinetic aggregate Agg1. As there is no sizeable energy barrier between monomer and Agg1, this process occurs spontaneously. By breaking the electrostatic interaction between counteranions (PF_6^-, ClO_4^-) and the metal complex cation, Agg1 (inactive nucleus) gradually transforms into Agg2 (active nucleus), which is an infinite linear M-M···M chain. This process is the rate-determining step during the self-assembly process and is highly dependent on the counteranion.

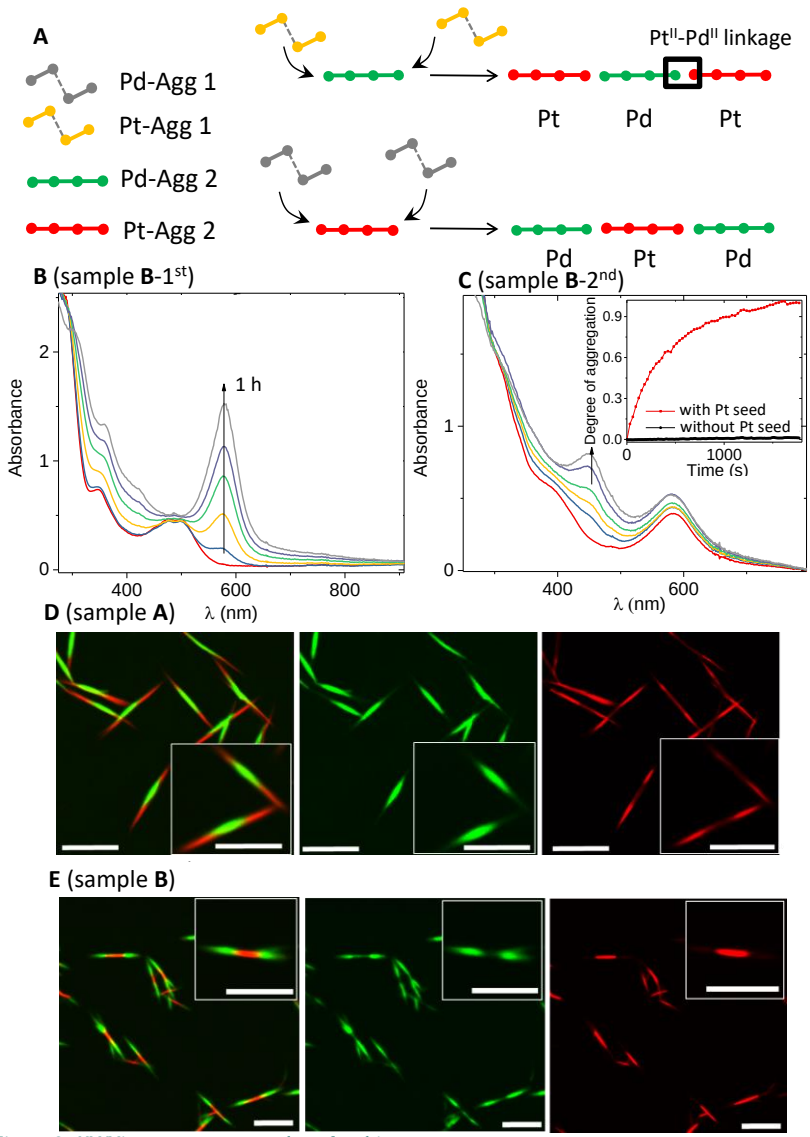

Figure 2. UV/Vis spectroscopy and confocal images.

(A) Schematic representation of the preparation of multi-block Pt^{II} and Pd^{II} supramolecular copolymers using a living supramolecular polymerization approach. (B) Time-dependent UV/Vis absorption spectral changes of **Pt-2-ClO$_4$** during the preparation of sample **B** in the 1st cycle. (C) Time-dependent UV/Vis absorption spectral changes of **Pd-1-ClO$_4$** during the preparation of sample **B** in the 2nd cycle. Inset: degree of aggregation for **Pd-1-ClO$_4$** with and without the addition of a **Pt-2-ClO$_4$** seed during the 2nd cycle in a time course (calculated from the absorbance at 439 nm). (D) Confocal images of the triblock red-green-red copolymers, sample **A**. From left to right: merged channel, green channel and red channel. (E) Confocal images of the triblock green-red-green copolymers, sample **B**. From left to right: merged channel, green channel and red channel. Details of the syntheses of samples **A** and **B** are provided in the supplemental experimental procedures. Scale bar: 8 μm.

Importantly, we found that Agg2 species of Pt^{II} or Pd^{II} complexes could be utilized as a seed to help metal complexes in the Agg1 state convert to the Agg2 state, as depicted in Figure 2A. Red-green-red triblock supramolecular copolymers (sample **A**, Figure 2D) were synthesized by using the **Pd-1-ClO$_4$** complex at the Agg2 state as a seed to initiate the transformation of the **Pt-2-ClO$_4$** complex from Agg1 to Agg2 state. Sample **A** in the 1st cycle was prepared by adding 1.9 mL of H_2O to a 100 μL CH_3CN solution of the **Pd-1-ClO$_4$** complex (3 mM), and the transformation from the Agg1 state to the Agg2 state took approximately one hour to complete. In the 2nd cycle, after 1 mL of freshly prepared **Pt-2-ClO$_4$** (H_2O/CH_3CN = 90:10 v/v, 1.0 × 10^{-4} M) in the Agg1 state was added to 1 mL of **Pd-1-ClO$_4$** seed solution, sample A was formed within 1.5 h. Time-dependent UV/Vis absorption and emission spectra were measured for sample **A** during the 1st and 2nd cycles, and they

showed that the **Pd-1-ClO$_4$** seed induced the transformation of the **Pt-2-ClO$_4$** complex to the Agg2 state (Figures S5-S6). Green-red-green triblock copolymers (sample **B**, Figure 2E) could be synthesized with a similar procedure using **Pt-2-ClO$_4$** in the Agg2 state as a seed. The **Pt-2-ClO$_4$** seed (Agg2) was prepared at a concentration of 1.5×10^{-4} M in H_2O/CH_3CN (95:5 v/v). As depicted in Figure 2C, without the addition of the **Pt-2-ClO$_4$** seed, **Pd-1-ClO$_4$** complex showed no time-dependent absorption spectral change within one hour, indicating that the **Pt-2-ClO$_4$** seed played a key role in initiating the transformation of **Pd-1-ClO$_4$** complex from Agg1 to Agg2 state. The structures of Agg1 and Agg2 provide useful insight into the mechanism with regard to the seed-induced self-assembly process. In X-ray crystal structures used for the model of metal complexes at Agg1 state (Figure 1A), the counteranions have close contact with the metal complex cation and block extended intermolecular M-M···M interactions, therefore preventing monomers from further aggregating at the ends of Agg1. Thus, Agg1 could be regarded as a kinetic trap state that prevents spontaneous aggregation during the self-assembly process. In contrast, no counteranion exists between the two metal complex cations of Pt^{II} or Pd^{II} complexes in the Agg2 state, where the crystal structures show infinite M-M···M intermolecular interactions (Figure 1A). Therefore, Agg2 could be used as an 'active' seed to initiate the aggregation of Pt^{II} or Pd^{II} complexes to form an elongated M-M···M chain structure. TEM-EDX (transmission electron microscopy energy-dispersive X-ray) mapping of platinum and palladium was used to characterize the multi-block Pt^{II} and Pd^{II} copolymer structures with relatively small sizes (Figures S8-S9). These block copolymers made of Pt^{II} and Pd^{II} complexes were found to be stable in water for a week; decomposition of Pt^{II} or Pd^{II} blocks or Pt^{II}-Pd^{II} linkages (Figure 2A) was not observed. Temperature-dependent UV/Vis spectroscopy measurements were performed on a Pt^{II}-Pd^{II}-Pt^{II} block copolymer sample to investigate the self-assembly mechanism (Figures S10-S13). ΔH (enthalpy release during the elongation process) and T_e (elongation temperature) values were obtained for the Pd^{II} inner-block and Pt^{II} outer-block of the Pt^{II}-Pd^{II}-Pt^{II} block copolymer sample, and the values were compared to those of the respective homopolymers.[50] The results indicated that the Pd^{II} inner-block component is stabilized upon forming the Pt^{II}-Pd^{II}-Pt^{II} block copolymer, as ΔH changed from -4.9 kcal/mol for the Pd homopolymer to -8.8 kcal/mol for the Pd inner-block (Table S2).

Control over the multi-block supramolecular copolymer structures in one and multiple dimensions

Both one- and multi-dimensional living supramolecular polymerization processes were achieved by varying the experimental conditions. Figure 3-4 shows the preparation process (monitored by UV/Vis absorption and emission spectroscopy) and confocal images of a 1D 5-block (red-green-yellow-green-red, sample **C**, three-step synthesis) and a 7-block (green-red-green-red-green-red-green, sample **D**, four-step synthesis) copolymer.

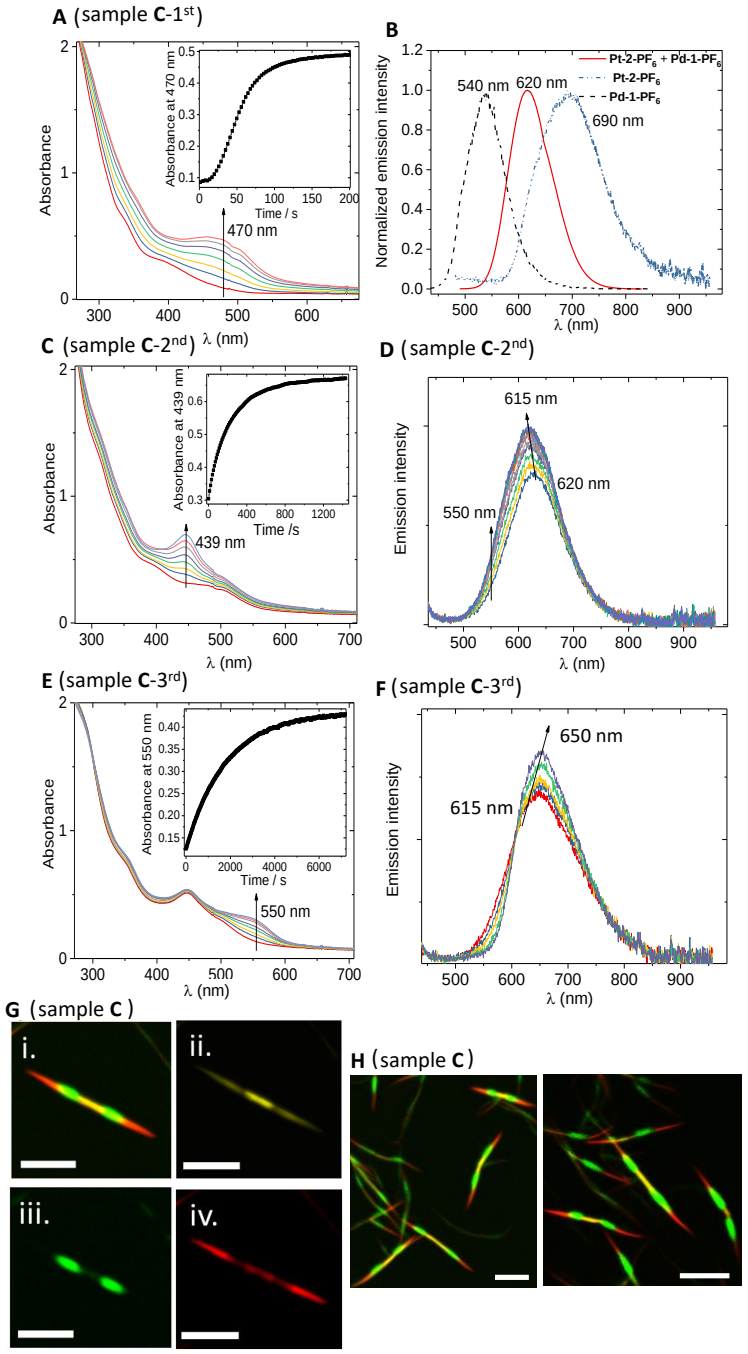

Figure 3. UV/Vis absorption and emission spectral changes and confocal images.
(A, C, E) Time-dependent UV/Vis absorption spectral changes of (A) sample **C**-1st, (C) sample **C**-2nd and (E) sample **C**-3rd. Inset in (A, C, E): Time-dependent absorbance changes of (A) sample **C**-1st at 470 nm, (C) sample **C**-2nd at 439 nm and (E) sample **C**-3rd at 550 nm. (B) Normalized emission spectra of **Pd-1-PF$_6$**, **Pt-2-PF$_6$** and the yellow-light-emitting seed (**Pd-1-PF$_6$** + **Pt-2-PF$_6$**) in the Agg2 state. (D, F) Time-dependent emission spectral changes of (D) sample **C**-2nd and (F) sample **C**-3rd. (G) Confocal images of sample **C**. i: merged channel, ii: yellow channel, iii: green channel and iv: red channel. (H) Confocal images of sample **C** in the merged channel. Details of the syntheses of samples **C** are provided in the supplemental experimental procedures. Scale bar: 5 μm.

The mixture of Pd^{II} and Pt^{II} complexes could undergo a co-assembly process with the Pt^{II}-Pd^{II} co-assemblies displaying various emission energies when the mixture ratio was changed (Figures S14-S15).[51] The yellow-light-emitting seed used for the synthesis of the 5-block copolymer was prepared by first mixing CH_3CN solutions of **Pd-1-PF$_6$** (200 μL) and **Pt-**

2-PF$_6$ (100 μL) at a concentration of 1 mM and then adding 1.7 mL of H_2O to their CH_3CN solution to induce the co-assembly process (sample **C**-1st, Figure 3A). The emission peaks of **Pd-1-PF$_6$** and **Pt-2-PF$_6$** in the Agg2 state were at 540 nm and 690 nm, respectively. A mixture of **Pd-1-PF$_6$** and **Pt-2-PF$_6$** in a 2:1 ratio exhibited a broad emission band at 620 nm (Figure 3B) at aggregate state. In the literature, oligo(phenylene ethynylene) (OPE)-based dichloro(bis)pyridyl Pt^{II} and Pd^{II} complexes were reported to display intriguing self-sorting behaviours and undergo an efficient statistical co-assembly process.[43] We performed temperature-dependent UV/Vis absorption spectroscopy measurements on the yellow-light-emitting seed prepared in the 1st step to investigate its self-assembly mechanism (Figure S17). A nonsigmoidal transition appeared, and an elongation temperature (T_e) of 333 K was determined from a plot of the fraction of aggregated species versus temperature, which is indicative of a co-nucleation process for the Pt^{II} and Pd^{II} complexes. The lag time shown in the inset of Figure 3A further indicates the existence of a Pt-Pd co-nucleus kinetically formed during the supramolecular polymerization. After **Pd-1-ClO$_4$** complex (at Agg1 state) was added to the solution containing the yellow-light-emitting seed prepared in the 1st step, a gradual increase in an absorption band at approximately 439 nm was observed without a lag time (Figure 3C), indicating the self-assembly of the **Pd-1-ClO$_4$** complex at the end of the seed. At the same time, the emission band at 620 nm became broader and blue-shifted to approximately 615 nm with increased emission intensity at ~550 nm (Figure 3D). During the preparation of sample **C** at the 3rd cycle by the addition of the **Pt-2-ClO$_4$** complex to a **C**-2nd solution, an absorption peak at approximately 550 nm gradually appeared without lag, and the emission band red-shifted to approximately 650 nm, indicating elongation of the **Pt-2-ClO$_4$** block (Figure 3E-F). Confocal images of sample **C** were obtained with observation windows of 650–770 nm, 470–550 nm and 570–630 nm (Figure 3G-H). The number-average length (L_n) of the assemblies in sample **C** was determined to be 2.2 μm, 6.5 μm and 11.7 μm in the 1st, 2nd and 3rd cycles, respectively (Figure S20).

The 7-block supramolecular copolymer (sample **D**, Figure 4) was synthesized using a seed prepared from **Pt-2-PF$_6$** (sample **D-1st**, 1×10^{-4} M, H_2O/CH_3CN, 85:15 v/v, Figure 4A). Adding 1 mL of the freshly prepared solution containing the **Pd-1-ClO$_4$** complex in the Agg1 state (1.5×10^{-4} M, H_2O/CH_3CN, 95:5 v/v) to 1 mL of sample **D-1st** (**Pt-2-PF$_6$** seed solution) resulted in gradual appearance of an absorption band at 439 nm within 10 min (sample **D-2nd**, Figure 4B). Subsequently, 1 mL of freshly prepared solution of the **Pt-2-ClO$_4$** complex in the Agg1 state (1×10^{-4} M, H_2O/CH_3CN, 90:10 v/v) was added to 1 mL of sample **D-2nd**, resulting in an absorption band at ~560 nm appearing within 20 min (sample **D-3rd**, Figure 4C). Finally, a 1 mL solution of the **Pd-1-ClO$_4$** complex in the Agg1 state (1.5×10^{-4} M, H_2O/CH_3CN, 95:5 v/v) was added to a 1 mL solution of sample **D-3rd** (Figure 4D), which led to the formation of a sequential 7-block supramolecular copolymer; the L_n[27] of the assemblies was determined to be 1.3 μm, 2.9 μm, 6.0 μm and 12.7 μm in the 1st, 2nd, 3rd and 4th cycles, respectively (Figure 4G). A narrow polydispersity was retained after each cycle during the living supramolecular polymerization, and the PDI of the self-assemblies in sample **D** was calculated to be 1.06, 1.02, 1.01 and 1.02 in the 1st, 2nd, 3rd and 4th cycles, respectively.

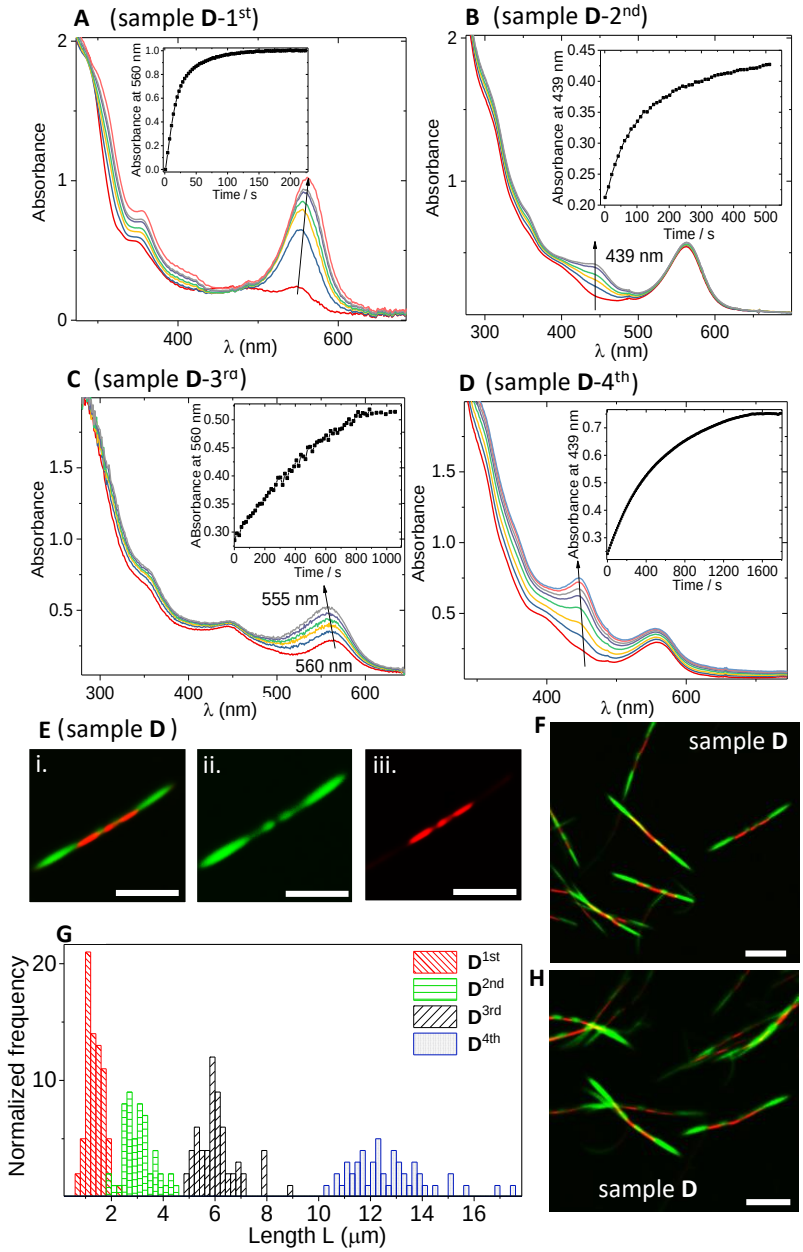

Figure 4. UV/Vis absorption spectral changes, histogram and confocal images.

(A-D) Time-dependent UV/Vis absorption spectral changes of (A) sample **D**-1st, (B) sample **D**-2nd, (C) sample **D**-3rd and (D) sample **D**-4th. Inset in (A-D): time-dependent absorbance changes of (A) sample **D**-1st at 560 nm, (B) sample **D**-2nd at 439 nm, (C) sample **D**-3rd at 560 nm and (D) sample **D**-4th at 439 nm. (E) Confocal images of sample **D**. i: merged channel, ii: green channel, iii: red channel. (F, H) Confocal images of sample **D** in the merged channel. (G) Length histogram of the assemblies of sample **D** for each cycle. Details of the syntheses of samples **C** and **D** are provided in the supplemental experimental procedures. Scale bar: 5 μm.

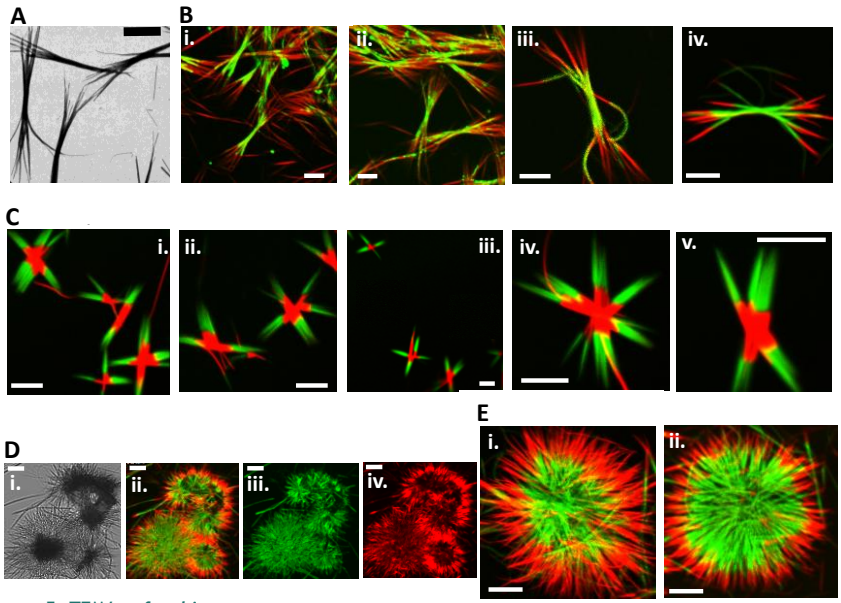

Figure 5. TEM/confocal images.

(A) TEM images of sample **E**. (B) Confocal images of sample **E**. (C) Confocal images of sample **F**. (D) Confocal images of sample **G** in the i: bright field, ii: merged channel, iii: green channel, and iv: red channel. (E) Confocal images of sample **G** in the merged channel. Details of the syntheses of samples **E**-**G** are provided in the supplemental experiment procedures. Scale bar: 5 μm.

The preparation of block supramolecular copolymers in multiple dimensions remains a great challenge.[8,25,52,53] Through kinetic control, we found that the living supramolecular polymerization of pincer Pt^{II} and Pd^{II} complexes could be achieved in two or even multiple dimensions. In our recent work, we prepared multi-dimensional non-symmetric nanostructures based on a series of cationic pincer-type Au^{III} complexes by changing the counteranions or concentration of the complex during their kinetically controlled self-assembly.[54] In this work, we found that changing the water content or temperature during the self-assembly process also led to the generation of multi-dimensional aggregate structures with these pincer-type cationic Pt^{II} or Pd^{II} complexes. By applying seeds having multi-dimensional aggregate structures, multi-dimensional block Pt^{II} and Pd^{II} supramolecular copolymers could be synthesized. Figure 5 shows confocal images of the triblock bowknot-shaped copolymer **E**, triblock star-shaped copolymer **F**, and triblock flower-shaped copolymer **G**. A multi-dimensional green-light-emitting seed of sample **E**-1^{st} was prepared through the self-assembly of **Pd-1**-ClO_4 in solution with 90% water content. For comparison, 95% water content was used in making the one-dimensional **Pd-1**-ClO_4 seed in sample **A**-1^{st}. The preparation of a multi-dimensional **Pt-2**-PF_6 seed of sample **F**-1^{st} was achieved by controlling the self-assembly process at a relatively high temperature of 303 K. For comparison, the one-dimensional **Pt-2**-PF_6 seed in sample **D**-1^{st} was synthesized at 298 K. Details of the syntheses of samples **E**-**G** are provided in the experimental procedures in supplementary information.

Increasing the temperature or decreasing the water content during the supramolecular polymerization process considerably decelerated the transformation of **Pt-2**-PF_6 from the Agg1 state to the Agg2 state, as reflected by the prolonged lag time shown in Figure 6A-B, leading to elongated polymers and significant changes in the morphology of the self-assemblies (Figure S21 and Figure 6C-E). Decreasing the concentration also remarkably slowed down the rate of the self-assembly, and the size of the aggregates increased (Figure S21).

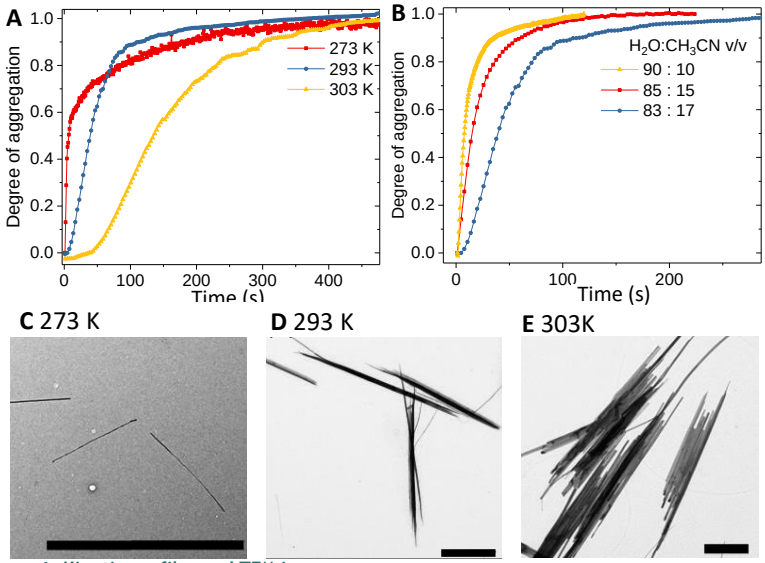

Figure 6. Kinetic profiles and TEM images.

Time-dependent degree of aggregation of **Pt-2-PF$_6$** (calculated from the absorbance at 560 nm in the UV/Vis absorption spectra) conducted at (A) different temperatures (H_2O/CH_3CN, 83:17 v/v, 1×10^{-4} M) and (B) different ratios of H_2O/CH_3CN (1×10^{-4} M) at 298 K. (C-E) TEM images of the polymer of **Pt-2-PF$_6$** in the Agg2 state obtained at 273 K (C), 293 K (D) and 303 K (E). Scale bar: 2 μm.

To describe the mechanism of kinetic control over supramolecular polymerization, we applied a model in which monomers were successively added to the previously aggregated fragments:[48,54-56]

Nucleation $2A \underset{k_-^a}{\overset{k^a}{\rightleftharpoons}} A_2 \underset{k_-^a}{\overset{k^a}{\rightleftharpoons}} A_i \cdots \underset{k_-^a}{\overset{k^a}{\rightleftharpoons}} A^*_{n-1} \underset{k_-^*}{\overset{k^*}{\rightleftharpoons}} A_n$ (1)

On-pathway, elongation of Agg2 $A_n \underset{k_-}{\overset{k}{\rightleftharpoons}} A_{n+1} \cdots \underset{k_-}{\overset{k}{\rightleftharpoons}} A_s$ (2)

Nucleation $2A \underset{k_-^a}{\overset{k^a}{\rightleftharpoons}} A_2 \underset{-A,k_-^a}{\overset{+A,k^a}{\rightleftharpoons}} A_3 \cdots A_i \cdots A_{n-2} \underset{-A,k_-^a}{\overset{+A,k^a}{\rightleftharpoons}} A^*_{n-1} \underset{k_-^*}{\overset{k^*}{\rightleftharpoons}} A_n$

On-pathway, elongation of Agg2 $A_n \underset{-A,k_-}{\overset{+A,k}{\rightleftharpoons}} A_{n+1} \cdots A_{s-1} \underset{-A,k_-}{\overset{+A,k}{\rightleftharpoons}} A_s$

Off-pathway, kinetic trap of Agg1 $A^*_{n-1} \underset{+A,k^a}{\overset{-A,k_-^a}{\rightleftharpoons}} A_{n-2} \underset{+A,k^a}{\overset{-A,k_-^a}{\rightleftharpoons}} A_{n-3} \cdots A_i \cdots A_2 \underset{k^a}{\overset{k_-^a}{\rightleftharpoons}} 2A_1$

Nucleation $2A \underset{k_-^a}{\overset{k^a}{\rightleftharpoons}} A_2 \underset{-A,k_-^a}{\overset{+A,k^a}{\rightleftharpoons}} A_3 \cdots A_i \cdots A_{n-2} \underset{-A,k_-^a}{\overset{+A,k^a}{\rightleftharpoons}} A^*_{n-1} \underset{k_-^*}{\overset{k^*}{\rightleftharpoons}} A_n$

On-pathway, elongation of Agg2 $A_n \underset{-A,k_-}{\overset{+A,k}{\rightleftharpoons}} A_{n+1} \cdots A_{s-1} \underset{-A,k_-}{\overset{+A,k}{\rightleftharpoons}} A_s$

Off-pathway, kinetic trap of Agg1 $A^*_{n-1} \underset{+A,k^a}{\overset{-A,k_-^a}{\rightleftharpoons}} A_{n-2} \underset{+A,k^a}{\overset{-A,k_-^a}{\rightleftharpoons}} A_{n-3} \cdots A_i \cdots A_2 \underset{k^a}{\overset{k_-^a}{\rightleftharpoons}} 2A_1$

Rate-determining step

Nucleation $2A \underset{k_-^a}{\overset{k^a}{\rightleftharpoons}} A_2 \underset{k_-^a}{\overset{k^a}{\rightleftharpoons}} A_i \cdots \underset{k_-^a}{\overset{k^a}{\rightleftharpoons}} A^*_{n-1} \underset{k_-^*}{\overset{k^*}{\rightleftharpoons}} A_n$ (1)

On-pathway, elongation of Agg2 $A_n \underset{k_-}{\overset{k}{\rightleftharpoons}} A_{n+1} \cdots \underset{k_-}{\overset{k}{\rightleftharpoons}} A_s$ (2)

Off-pathway, kinetic trap of Agg1 $A^*_{n-1} \underset{k^a}{\overset{k_-^a}{\rightleftharpoons}} A_{n-2} \underset{k^a}{\overset{k_-^a}{\rightleftharpoons}} A_i \cdots A_2 \underset{k^a}{\overset{k_-^a}{\rightleftharpoons}} 2A$ (3)

where *A* represents the Pt or Pd monomers; k^a and k_-^a represent the rate constants of the formation and dissociation of A_i (A_i represents the aggregates having i-mers, i < n),

respectively; $A^*_{n-1} \rightarrow A_n$ represents the transformation from Agg1 state to Agg2 state (equation 1) that occurs due to the breaking of counteranion-cation interaction; k^* and k_-^* represent the rate constants of the formation and dissociation of A_n, respectively; and k and k_- are the rate constants of the forward and reverse chain elongation reactions, respectively (equation 2). During the synthesis of block Pt^{II} and Pd^{II} copolymers, a seed A_n (Pt^{II} or Pd^{II} complex at Agg2) prepared in advance is directly added to the solution containing A^*_{n-1} (Pd^{II} or Pt^{II} complex in the Agg1 state). Monomers are quickly consumed during the elongation process (equation 2), leading to depolymerization of Agg1 (equation 3). Therefore, a block Pt^{II} and Pd^{II} copolymer could be obtained through the gradual elongation of Pt^{II} or Pd^{II} complexes at the end of the Pd^{II} or Pt^{II} seed.

The rate of the formation of A_n could be expressed as:

$$\frac{d[A_n]}{dt} = k^*[A][A^*_{n-1}] - k_-^*[A_n] - k[A][A_n] + k_-[A_{n+1}] \quad (4)$$

where $[A]$, $[A_n]$, $[A^*_{n-1}]$ and $[A_{n+1}]$ represent the concentrations of monomer A, nucleus A_n, A^*_{n-1} and elongated polymer A_{n+1}. Equation (4) indicates that the key parameters in determining the initial formation rate of A_n (Agg2) are $[A]$, $[A^*_{n-1}]$ and k^* ($[A_n] = [A_{n+1}] = 0$ during the lag period). Herein, we used the model described in equations (1-4) to explain the relationships between the kinetics, aggregate size, growth direction and the temperature, water-content, concentration of complexes, counteranions during the self-assembly process.

(1) Temperature-dependent kinetics: temperature influences the degree of aggregation (α) of complexes in the Agg1 or Agg2 stages during the self-assembly process. With the temperature increasing from 273 K to 303 K, an increasing number of monomers remain in the solution and in equilibrium with Agg1 (Figure 1E) during the lag time. Depolymerisation of A^*_{n-1} would be relatively fast, and $[A^*_{n-1}]$ would decrease, leading to a relatively slow transformation from Agg1 to Agg2. Part of the complexes at the end of the nucleus would be activated gradually, while part of the complexes would be trapped in the Agg1 state due to the slowness of the $A^*_{n-1} \rightarrow A_n$ transformation. The remaining monomers could only aggregate at the end of the activated nucleus (Agg2) site while could not grow at the end of the Agg1 site, leading to the formation of multi-dimensional structures. On the other hand, according to Figure 1E, the α of **Pt-2-PF_6** in the Agg1 state decreased, while the α of **Pt-2-PF_6** in the Agg2 state was slightly influenced when the temperature was increased from 293 K to 303 K. Therefore, at 303 K, many monomers remained in equilibrium with Agg1 during the lag period (before the formation of A_n), while most of the monomers were consumed and formed Agg2 during the elongation process (after the formation of A_n). In summary, the supramolecular polymerization conducted at 303 K (Figure 6E) resulted in larger self-assemblies during the elongation process because fewer nuclei A_n and more monomer formed before elongation in the solution at 303 K than at 293 K.

(2) Water content-dependent kinetics: the water content of solutions also influences the α of the complexes. With decreasing water content, α decreases (no aggregate of Pt^{II} or Pd^{II} complexes is observed in the UV/Vis spectrum when the water content is below 30%), and many monomers remain in the solution. Consequently, a relatively low concentration of A^*_{n-1} leads to a slow transformation from Agg1 to Agg2 and multi-dimensional growth (similar case of the temperature-dependent kinetics). More monomer and fewer nuclei (A_n) in low-water solutions than in high-water solutions leads to the generation of larger self-assemblies in the low-water solutions.

(3) Concentration- and counteranion-dependent kinetics: According to equation (4), the rate of the formation of active nucleus A_n is proportional to the concentration of monomer A. Therefore, decreasing the concentration of complexes would slow the formation of A_n, leading to the existence of more monomer and less A_n at relatively low concentrations. Consequently, the formation of increased aggregate sizes has been observed (Figure S21). Changes in the counteranion mainly influence k^* and k_-^*, which are affected by the interaction strength between the complex cation and the counteranion.[54] The kinetic barrier during supramolecular polymerization is much higher for complexes with ClO_4^- as a counteranion than for those with PF_6^-, leading to a relatively slow Agg1→Agg2

transformation for the M-ClO_4^- (M = Pt^{II} or Pd^{II}) complexes during supramolecular polymerization (Figure 1D).[55]

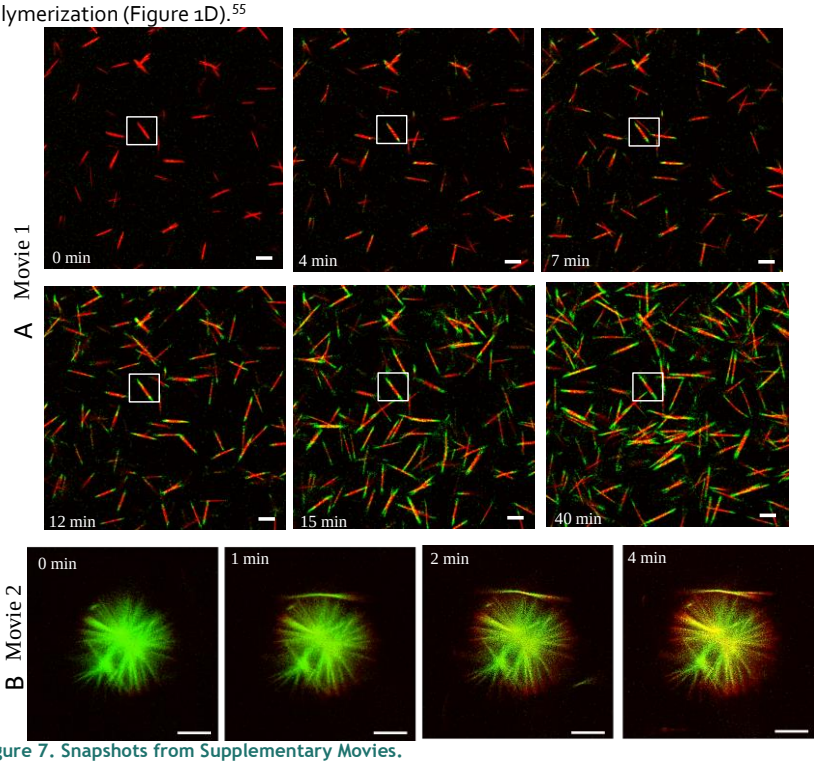

Figure 7. Snapshots from Supplementary Movies.
(A) Real-time evolution of the elongation process of the **Pd-1-ClO_4** complex at the end of a **Pt-2-ClO_4** seed in Supplementary Movie 1. (B) Real-time evolution of the elongation process of the **Pt-2-ClO_4** complex around a **Pd-1-ClO_4** seed in Supplementary Movie 2. Details of the preparation of Movie 1 and 2 are provided in the supplemental experiment procedures. Scale bar: 10 μm.

To monitor the dynamic elongation process during the living supramolecular polymerization of Pt^{II} and Pd^{II} complexes, we performed real-time imaging of the evolution using confocal microscopy. First, we prepared a one-dimensional **Pt-2-ClO_4** red-light-emitting seed at a concentration of 1.5×10^{-4} M and a multi-dimensional green-light-emitting **Pd-1-ClO_4** seed at a concentration of 1×10^{-4} M. These freshly prepared seeds (50 μL) were drop-casted onto a glass bottom dish, which was followed by the addition of 50 μL of **Pd-1-ClO_4** or **Pt-2-ClO_4** in the Agg1 state at a concentration of 1×10^{-4} M. The results are displayed in Figure 7 and Supplementary Movie 1 and 2. As depicted in Movie 1 (Figure 7A), upon the addition of Pd-Agg1 into a solution containing the Pt-Agg2 seed, a gradual elongation of **Pd-1-ClO_4** block was recorded. During the elongation process, the Pd complex in the Agg1 state gradually depolymerized to monomers and transformed to the Agg2 state at the end of the Pt seed. Therefore, a gradual elongation of the **Pd-1-ClO_4** block at the end of the red-light-emitting **Pt-2-ClO_4** seed was observed in confocal images. Similarly, a gradual elongation process of the **Pt-2-ClO_4** block around the **Pd-1-ClO_4** seed was observed in Movie 2 (Figure 7B).

Amplified phosphorescence efficiency in the Pt^{II} complex-doped Pd^{II} assemblies

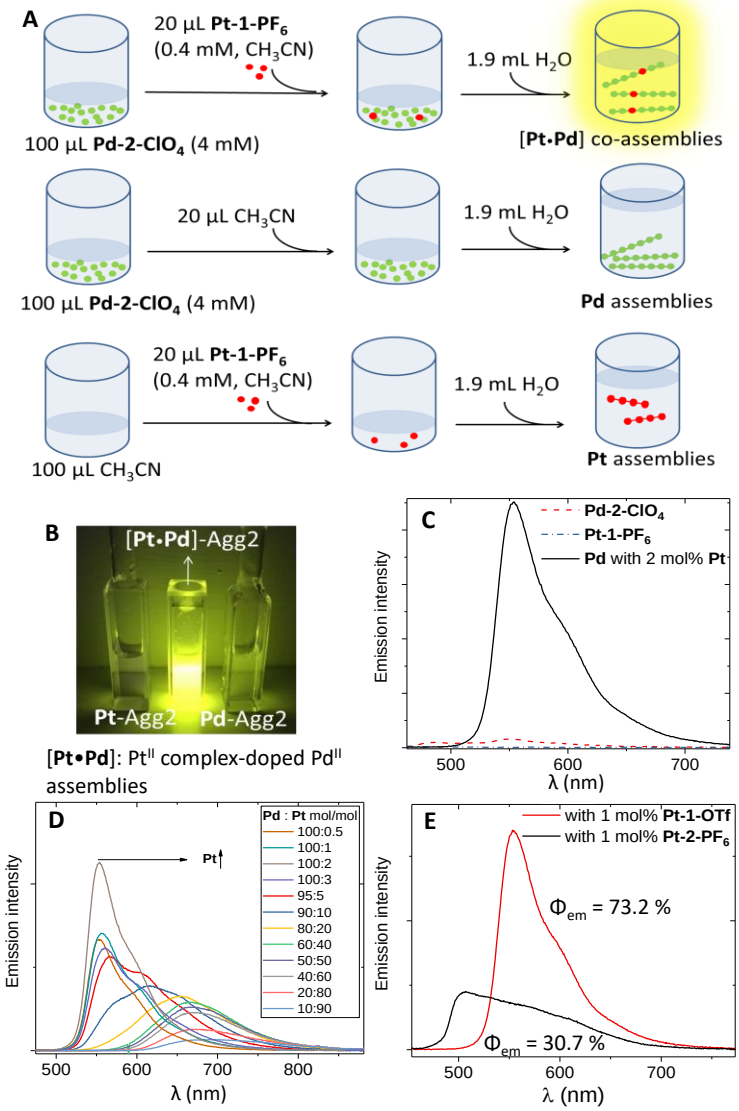

Figure 8. Preparation procedures and emission spectra.

(A) Preparation of the [**Pt·Pd**] co-assemblies (**Pd-2-ClO$_4$** with 2 mol% **Pt-1-PF$_6$**), **Pd-2-ClO$_4$** assemblies and **Pt-1-PF$_6$** assemblies (from top to bottom). (B) Emission colour of [**Pt·Pd**] co-assemblies, **Pd-2-ClO$_4$** assemblies and **Pt-1-PF$_6$** assemblies (λ_{ex} = 365 nm) in the Agg2 state obtained using the preparation procedure described in (A). (C) Emission spectra for [**Pt·Pd**] co-assemblies (**Pd-2-ClO$_4$** with 2 mol% **Pt-1-PF$_6$**), **Pd-2-ClO$_4$** assemblies and **Pt-1-PF$_6$** assemblies in the Agg2 state obtained using the preparation procedure described in (A). (D) Emission spectra for [**Pt·Pd**] co-assemblies in the Agg2 state obtained with different doping ratios of **Pt-1-PF$_6$**. (E) Emission spectra for [**Pd-2-ClO$_4$·Pt-2-PF$_6$**] and [**Pd-2-ClO$_4$· Pt-1-OTf**] co-assemblies doped with 1 mol% Pt complex.

In addition to the controlled synthesis of sequential block Pt^{II} and Pd^{II} supramolecular copolymers in one and multiple dimensions, we also successfully synthesized strongly phosphorescent [**Pt•Pd**] co-assemblies by doping a small amount of Pt^{II} complexes into the Pd^{II} assemblies during the supramolecular polymerization. We found that the supramolecular co-assemblies prepared from the mixture of Pd^{II} assemblies and the Pt^{II} complexes showed high phosphorescence emission efficiencies. Further studies revealed that mixing a small amount of the **Pt-1-PF$_6$** complex (0.5 mol%, 1 mol%, 2 mol%, 3 mol%, in Table S3) into the **Pd-2-ClO$_4$** complex and subsequently inducing the co-assembly process changed the emission quantum yield from ~3.7% in Pd assemblies (without doping) to 60.6% (Figure S22), 70.3%, 76.2% (Figure S23), and 71.3% within one hour, respectively, in the resulting Pt^{II} complex-doped Pd^{II} assemblies [**Pt•Pd**] (note that **Pt-1-PF$_6$** displayed weak

emission in the Agg2 state at a concentration of 4×10^{-6} M, as shown in Figure 8B-C). The emission energy red-shifted with a further increasing doping ratio of the Pt complex (Figure 8D). Replacing **Pt-1-PF$_6$** with other pincer-type Pt^{II} complexes (**Pt-1-OTf**, **Pt-2-PF$_6$**) resulted in similar emission intensity enhancement and shift in emission energy, as shown in Figure 8E (note that **Pt-1-OTf** or **Pt-2-PF$_6$** displayed weak emission in the Agg2 state at a concentration of 2×10^{-6} M). Such a Pt^{II} complex-induced emission enhancement was also observed for other pincer-type Pd^{II} emitters studied in this work (Figures S24-S26) but not for Pd^{II} complexes with OTf^- as the counteranion (Figure S27).

Time-dependent emission quantum yields and spectral changes of **Pt-1-PF$_6$** assemblies, **Pd-2-ClO$_4$** assemblies and [**Pt•Pd**] co-assemblies (Pt^{II} complex-doped Pd^{II} assemblies) were monitored at different time intervals, as shown in Figure 9A-C. For complex **Pd-2-ClO$_4$**, with the transformation from the kinetic aggregate (Agg1) to the thermodynamic aggregate (Agg2), two emission bands at approximately 485 nm and 550 nm gradually appeared with weak emission intensity and an emission lifetime of 2.1 μs. For complex **Pt-1-PF$_6$**, a broad emission band at approximately 720 nm appeared upon aggregation (1×10^{-4} M, H_2O/CH_3CN, 90:10 v/v) and exhibited a relatively short emission lifetime of 0.12 μs and an emission quantum yield of 13%. In contrast, a broad emission band at 550 nm developed over time for [**Pt•Pd**] co-assemblies (1 mol% **Pt-1-PF$_6$**), with greatly enhanced emission efficiency (Φ_{em} of up to 70%) and an emission lifetime of 1.3 μs. The gradually increased emission intensity for [**Pt•Pd**] co-assemblies over time indicated that the Pt^{II} and Pd^{II} complexes were first trapped in a metastable kinetic state during co-assembly (Figure 9D). Nanosecond time-resolved emission spectra of [**Pt•Pd**] co-assemblies showed the decay of a single broad emission band with a peak maximum at ~550 nm on the microsecond timescale (Figure S28, for transient absorption spectra, see also Figures S29-S30). No emission band at 720 nm (from **Pt-1-PF$_6$** homopolymers) or 485 nm (from **Pd-2-ClO$_4$** homopolymers) was observed after photoexcitation, indicating that the co-assembly structure has a different emissive excited state from that of the homopolymers. To exclude the possibility that the enhanced emission is from the co-existence of Pd^{II} homopolymers and short Pd^{II} and/or Pt^{II} dimers/oligomers in solution, we performed control experiments to further show that the amplified emission is derived from the Pt complexes doped into the [**Pt•Pd**] co-assemblies. We added a small amount of 2 mol% **Pd-2-ClO$_4$** (20 μL, 0.4 mM) and/or **Pt-1-PF$_6$** (20 μL, 0.4 mM) into the Pd-homopolymer solution to form short dimers/oligomers, and no obvious amplified emission intensity was observed (Figure S31). Photo-physical data of [**Pt•Pd**] co-assemblies prepared by varying the doping ratio of **Pt-1-PF$_6$** are summarized in Table S3, and the measured emission quantum yield and lifetime are displayed in Figure 9E-F. The highest emission efficiency was realized by doping 2 mol% of **Pt-1-PF$_6$** into the **Pd-2-ClO$_4$** complex, where k_r increased dramatically from 1.8×10^4 s^{-1} to 58.6×10^4 s^{-1} and k_{nr} decreased from 45.8×10^4 s^{-1} to 18.3×10^4 s^{-1} in the change from **Pd-2-ClO$_4$** assemblies to [**Pt•Pd**] co-assemblies. The relative large k_r and small k_{nr} values altogether account for the high emission efficiencies of [**Pt•Pd**] co-assemblies. The k_{nr} constant increased when the doping ratio of **Pt-1-PF$_6$** was higher than 2 mol% (Table S3). The large k_{nr} leads to relatively low phosphorescence efficiency in [**Pt•Pd**] co-assemblies, as shown in Figure 9E, which could be accounted for by the energy gap law, as the emission energy showed a significant redshift in the copolymers with a high **Pt-1-PF$_6$** doping ratio (Figure 8D and Table S3).

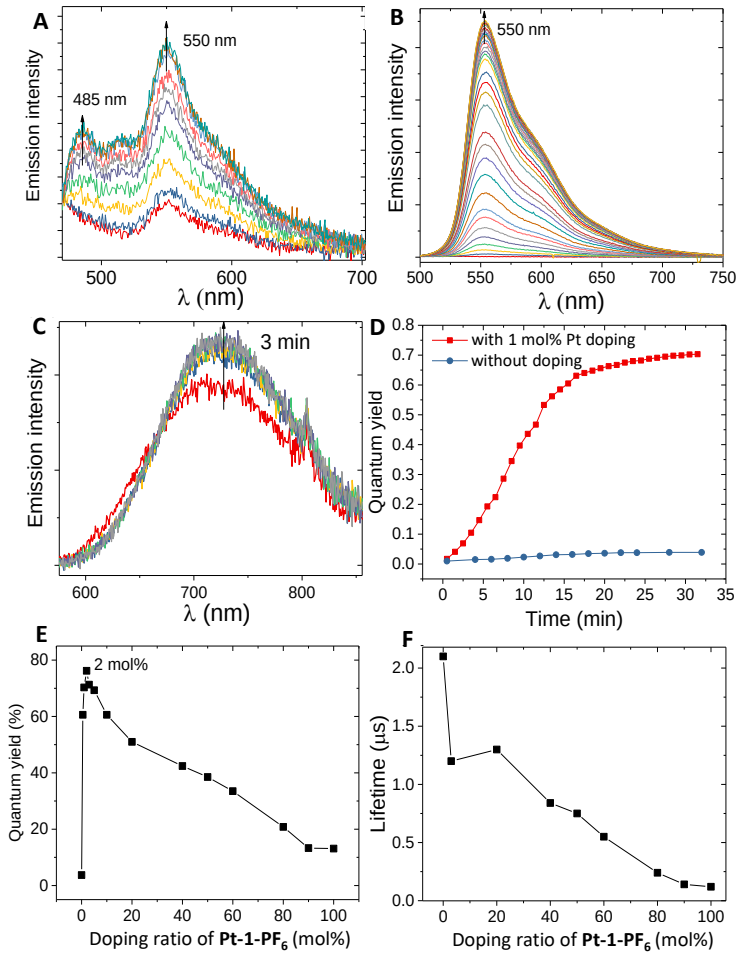

Figure 9. Time-dependent emission spectra and photo-physical data of the [Pt-1-PF_6•Pd-2-ClO_4] co-assemblies.

(A) Time-dependent emission spectral changes of **Pd-2-ClO_4** (H_2O/CH_3CN, 95:5 v/v, 2×10^{-4} M). (B) Time-dependent emission spectral changes of **Pd-2-ClO_4** (2×10^{-4} M) doped with 1 mol% **Pt-1-PF_6** in H_2O/CH_3CN (95:5 v/v). (C) Time-dependent emission spectral changes of **Pt-1-PF_6** (1×10^{-4} M) in H_2O/CH_3CN (90:10 v/v). (D) Time-dependent emission quantum yield change in **Pd-2-ClO_4** (H_2O/CH_3CN, 95:5 v/v, 2×10^{-4} M) without doping and with doping 1 mol% **Pt-1-PF_6** complex. (E) Emission quantum yield change in [**Pt-1-PF_6·Pd-2-ClO_4**] co-assemblies with different doping ratios of the **Pt-1-PF_6** complex. (F) Emission lifetime change in [**Pt-1-PF_6·Pd-2-ClO_4**] co-assemblies with different doping ratios of **Pt-1-PF_6**.

During co-assembly, extended metal-metal (M-M) contacts are formed between adjacent Pd^{II} and Pt^{II} complexes, leading to mixing of the Pt^{II} $5d_{z^2}$ orbital with Pd^{II} $4d_{z^2}$ orbital. Upon excitation of one electron from the dσ* orbital to a π* orbital of the ligand, a delocalized ^{3}MMLCT excited state is generated in the [**Pt•Pd**] co-assemblies; which has also been revealed by density functional theory (DFT) calculations. The optimized triplet excited-state geometry of the [**Pt-1•Pd-2**] dimer reveals a shortening of the Pt-Pd distance from 3.37 Å in the S_0 state to 2.92 Å in the T_1 state (Figure 10A), which supports the existence of attractive Pt-Pd interactions in the T_1 state. Figure 10B shows that both Pt and Pd atoms contribute to the dσ* orbital (for dimers and tetramers composed of **Pt-1** and **Pd-1**, see also Figures S32-S34), while the lowest unoccupied MO (LUMO) is mainly localized on the π* orbital of the ligand in **Pt-1-PF_6**.

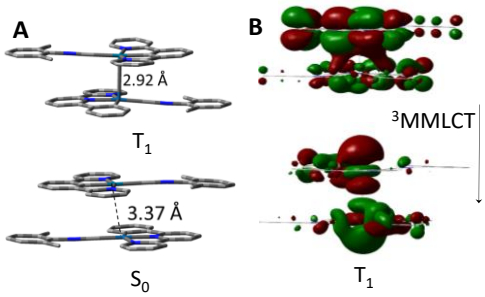

Figure 10. Optimized structures and MO diagram.

(A) Optimized structures of [**Pt-1**·**Pd-2**] in the S_0 and T_1 states. (B) Calculated molecular orbital (MO) diagram of [**Pt-1**·**Pd-2**] based on the optimized T_1 geometry using the time-dependent DFT (TDDFT) method. Complex **Pd-2** is at the bottom, and complex **Pt-1** is at the top.

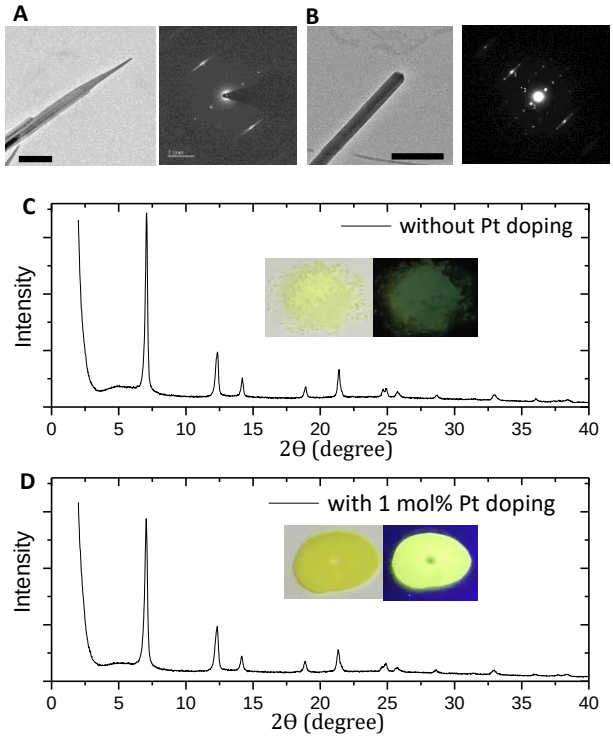

Figure 11. TEM images and powder XRD patterns.

(A-B) TEM images of **Pd-2-ClO$_4$** in the Agg2 state and its corresponding SAED patterns without doping in (A) and doped with 1 mol% **Pt-1-PF$_6$** in (B). Scale bar: 500 nm. (C-D) Powder XRD of the **Pd-2-ClO$_4$** complex in Agg2 without doping in (C) and doped with 1 mol% **Pt-1-PF$_6$** in (D). Inset: colour of the powder under (left) room lighting and (right) excitation at 365 nm.

We then carried out a microscopy study to examine whether the enhanced phosphorescence efficiency is related to the microscopic structures of the [**Pt•Pd**] co-assemblies obtained by doping of the Pt complex to the Pd assemblies. The phosphorescence efficiencies of the [**Pt•Pd**] co-assemblies were highly dependent on the co-assembly process: after a small amount of Pt complex (1 mol%) was doped into samples with a Pd complex, co-assemblies made from Pt-X$^-$(X = PF_6, ClO_4 or OTf) and Pd-X$^-$ (X = PF_6 or ClO_4) displayed greatly enhanced emissions, while one prepared from Pt-X$^-$(X = PF_6, ClO_4 or OTf) and Pd-OTf$^-$ showed only negligible emission in the aggregate state (Figure S27). The Agg1 state of the Pd-OTf$^-$ complex cannot transform to the Agg2 state in mixed H_2O/CH_3CN solvent, which is attributable to the relatively strong interaction between the

complex cation and OTf^-.[30] Therefore, we considered that the formation of the Agg2 state with extended Pt-Pd contacts was prohibited when Pd-OTf was used as the major component in the preparation of the Pt^{II}/Pd^{II} co-assemblies. A crystalline structure was observed for [**Pd-2-ClO$_4$·Pt-1-PF$_6$**], [**Pd-1-PF$_6$·Pt-1-PF$_6$**] and [**Pd-1-ClO$_4$·Pt-1-PF$_6$**] co-assemblies upon aggregation and characterized by selected area electron diffraction (SAED), powder X-ray diffraction (XRD) or X-ray crystal structure analyses. Sharp and ordered spots were observed in the SAED pattern of a single nanowire for both Pd assemblies and [**Pt•Pd**] co-assemblies (Figure 11A-B, see also Figures S35-S37), where a d spacing of 3.3-3.4 Å was calculated for the intermolecular distance and the growth direction of these nanowires was considered to be along the metal-metal chains[46]. In Figure 11C-D, XRD patterns of dried films of Pd assemblies and [**Pt•Pd**] co-assemblies obtained by centrifuging solutions containing the aggregates were compared: the packed forms of molecules in **Pd-2-ClO$_4$** assemblies resembled those in the [**Pt-1-PF$_6$·Pd-2-ClO$_4$**] co-assemblies, while the emission intensity showed distinct differences, as shown in the inset pictures. Both SAED and XRD patterns revealed that introducing a small amount of Pt complexes into Pd aggregates slightly or negligibly influenced the crystalline structure of the Pd assemblies. A highly ordered and regular co-crystalline [**Pt•Pd**] co-assembly was obtained through co-assembly. Moreover, we determined the structures of needle-like co-crystals of [**Pd-1-PF$_6$**]$_{0.89}$[**Pt-1-PF$_6$**]$_{0.11}$, [**Pd-1-PF$_6$**]$_{0.82}$[**Pt-1-PF$_6$**]$_{0.18}$, and [**Pd-1-PF$_6$**]$_{0.58}$[**Pt-1-PF$_6$**]$_{0.42}$. The structures of these three crystals feature infinite M-M···M chains with alternating M-M distances of 3.3 and 3.4 Å (Figure 12A, see also Figures S38-S40), similar to crystal structures reported for **Pd-1-PF$_6$** and **Pt-1-PF$_6$** in the literature.[30,46] The colour and emission energy showed a gradual redshift with an increasing mixture ratio of **Pt-1-PF$_6$**, as shown in Figure 12B-C, indicating an increased contribution of the Pt^{II} $5d_{z^2}$ orbitals to the excited state.

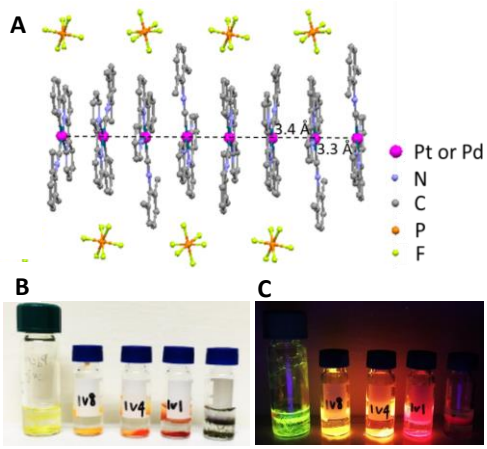

Figure 12. Crystal structure and colours.

(A) Crystal structure of [**Pd-1-PF$_6$**]$_{0.58}$[**Pt-1-PF$_6$**]$_{0.42}$ featuring an infinite 1D M-M chain structure (M = Pt or Pd). (B) Colours of crystals of **Pd-1-PF$_6$**, [**Pd-1-PF$_6$**]$_{0.89}$[**Pt-1-PF$_6$**]$_{0.11}$, [**Pd-1-PF$_6$**]$_{0.82}$[**Pt-1-PF$_6$**]$_{0.18}$, [**Pd-1-PF$_6$**]$_{0.58}$[**Pt-1-PF$_6$**]$_{0.42}$, and **Pt-1-PF$_6$** (from left to right) under room lighting. (C) Emission colour of crystals of **Pd-1-PF$_6$**, [**Pd-1-PF$_6$**]$_{0.89}$[**Pt-1-PF$_6$**]$_{0.11}$, [**Pd-1-PF$_6$**]$_{0.82}$[**Pt-1-PF$_6$**]$_{0.18}$, [**Pd-1-PF$_6$**]$_{0.58}$[**Pt-1-PF$_6$**]$_{0.42}$, and **Pt-1-PF$_6$** (from left to right) upon excitation at 365 nm.

Based on these spectroscopy and microscopy studies, the greatly enhanced phosphorescence intensity of the Pd aggregates by doping with a small amount of Pt complexes is attributed to the following factors: (1) An efficient kinetically controlled co-assembly process that is influenced by the transformation from a Pt^{II}-Pd^{II} co-Agg1 state to the co-Agg2 state (Figure 9B and 9D). The co-assembly process leads to co-crystalline structures (Figure 12) with Pt-Pd bonding interactions in the excited state[37] and a delocalized ^{3}MMLCT transition upon photoexcitation (Figure 10). (2) The k_r in [**Pt•Pd**] co-assemblies (Pt^{II} complex-doped Pd^{II} assemblies) showed a significant increase, while k_{nr} exhibited relatively small changes (k_r = 1.8 × 10^4 s^{-1}, k_{nr} = 45.8 × 10^4 s^{-1} in Pd^{II} assemblies; k_r = 54.1 × 10^4 s^{-1}, k_{nr} = 22.9 × 10^4 s^{-1} in [**Pt•Pd**] co-assemblies doped with 1 mol% Pt^{II} complexes, see Table S3). The microscopic structures of the [**Pt•Pd**] co-assemblies possess similar crystalline structures as the non-doped ones, indicating that the greatly enhanced

phosphorescence efficiencies have been mainly influenced by the increased k_r values. The cause of these changes is tentatively identified as the external heavy-atom spin-orbit coupling from Pt atoms[57,58]. In contrast to conventional cases showing external heavy-atom effect-facilitated phosphorescence, where a large amount of organic solvent (which usually contains heavy halogen atoms such as I and Br)[59] or a high concentration of a heavy-atom salt (KI or $TlNO_3$)[60,61] or noble metals in rare gas matrices (Au in Ar, Kr, and Xe)[62] were used, in this work, a small amount of Pt^{II} complexes was sufficient to induce external perturbation in the [**Pt•Pd**] co-assemblies. A theory accounting for the external heavy-atom effect suggested that the orbital overlap integral between external perturbation component and emissive component is one of the decisive factors in determining the spin-orbit splitting.[62] In principle, the Pt $5d_{z^2}$ orbital could mix with the Pd $4d_{z^2}$ orbital because they have the same symmetry, which renders a significant overlap integral between the external Pt^{II} complex and the emissive Pd^{II} complex, leading to considerable involvement of Pt orbitals in the frontier orbitals. Therefore, external Pt-atom perturbation is suggested to be responsible for the pathway promoting the $T_1 \rightarrow S_0$ radiative decay in the Pd assemblies, in which case the radiative decay of the phosphorescence would be accelerated with the significantly improved emission efficiency.

Another point we would like to address is that how many Pt and Pd molecules are involved into a delocalized ^{3}MMLCT excited state of the [**Pt•Pd**] co-assemblies upon photo-excitation. The single emission band at around 550 nm showed up (Figure 9A) and decayed with a lifetime of around 1.3 μs (Figure S29) for the **Pd-2-ClO$_4$** complex doped with 1 mol% **Pt-1-PF$_6$** complex. No emission band at ~485 nm (τ = 2.1 μs in **Pd-2-ClO$_4$**) or emission band at ~720 nm (τ = 0.12 μs in **Pt-1-PF$_6$**) has been observed, suggesting that ~100 **Pd-2-ClO$_4$** complexes and one **Pt-1-PF$_6$** complex could form a delocalized ^{3}MMLCT excited state on the average, where the HOMO is composed of the Pd-$4d_{z^2}$/Pt-$5d_{z^2}$ orbital and the LUMO is composed of the π* orbital of tridentate N^C^N/C^N^N ligand. Such a ^{3}MMLCT excited state delocalizing over the Pt and Pd complexes renders an emissive state having emission energy and lifetime different from that of respective **Pt-1-PF$_6$** and **Pd-2-ClO$_4$** homopolymers. The M-M···M distance is ~3.3 Å in the co-crystal structure of the Pt and Pd complex (Figure 12), giving the approximate length of the delocalized excited state of around 33 nm. In other words, the [**Pt•Pd**] co-assembly prepared by the doping approach could be regarded as a small block Pt and Pd copolymer at the molecular level, where its size falls into the range of the delocalization of an excited state and its emission comes from a distinctive ^{3}MMLCT transition involving both of the Pt and Pd complexes.

Conclusion

In conclusion, we have demonstrated the preparation of sequential phosphorescent multi-block supramolecular copolymers made using Pt^{II} and Pd^{II} complexes via a living supramolecular polymerization approach. The size, morphology and dimensions of the supramolecular block copolymers could be manipulated under kinetic control. The triplet-state emission energies and efficiencies of the Pd^{II} aggregates were greatly influenced by doping with a small amount of Pt^{II} complexes through a co-assembly process. The synthesis of 1D/2D block Pt^{II} and Pd^{II} supramolecular copolymers and the discovery of amplified phosphorescence efficiencies in the [**Pt•Pd**] co-assemblies will facilitate the exploration of potential applications for supramolecular polymeric materials.

EXPERIMENTAL PROCEDURES

Procedure of preparing the block Pt^{II} and Pd^{II} supramolecular copolymer

Addition of 1 mL of a seed solution (Agg2 of Pt^{II} or Pd^{II} complexes) to 1 mL of a solution containing an Agg1 species (Pd^{II} or Pt^{II} complex) resulted in the appearance of block Pd^{II} and Pt^{II} supramolecular copolymers without lag. Subsequently, 1 mL of the resultant supramolecular polymer solution was removed, and another 1 mL of freshly prepared solution containing the kinetic aggregates (Pd^{II} or Pt^{II} complex) was added to the remaining polymer solution. The procedures were repeated, and subsequent supramolecular polymerization occurred accordingly. Details of the synthesis and characterization of supramolecular copolymer samples **A**-**K** are included in the supplemental information (see also Figures S45-S53).

Procedure of preparing the [Pt•Pd] co-assemblies with enhanced phosphorescence:

To induce the co-assembly of the Pt^{II} and Pd^{II} supramolecular copolymers with amplified phosphorescence intensity, CH_3CN solutions of Pt^{II} and Pd^{II} complexes were first pre-mixed in different ratios, and then a specific amount of water was injected into the CH_3CN solution to trigger the co-assembly process.

DATA AVAILABILITY

CCDC number for the co-crystal structures reported in this paper is1918565-1918567.

SUPPLEMENTAL INFORMATION

Document S1. Supplemental Experimental Procedures and Computational Details, Figures S1–S60, and Table S1-S6

Movie 1. Real-time visualization of the growth of Pd-Pt-Pd block copolymer

Movie 2. Real-time visualization of the growth of Pt-Pd-Pt block copolymer

ACKNOWLEDGMENTS

We thank the support of Hong Kong Research Grants Council (HKU 17330416) and Basic Research Program-Shenzhen Fund (JCYJ20160229123546997, JCYJ20170412140251576, and JCYJ20170818141858021). This work was conducted in part using the research computing facilities and/or advisory services offered by Information Technology Services, The University of Hong Kong. We thank Mr. Ming Zhang for help in the confocal microscopy experiments. We thank Dr. Kam-Hung Low for the help in the PXRD measurement. We thank Dr. Zhiping Yan for the help with the femtosecond transient absorption spectroscopic measurement. We thank Mr. Chan Y. F. Frankie for the help in the TEM-EDX analysis. We thank Ms. Shuo Xu for the help with the measurement of the length of the block copolymers.

AUTHOR CONTRIBUTIONS

Conceptualization, Q. W. and C. -M. C.; Formal Analysis & Validation & Writing-Original Draft, Q. W. and C. -M. C.; Investigation, Q. W., W.-P. T. and X.C.; Writing-Review & Editing, Q. W., W.-P. T. and C. -M. C.; Supervision & Resources, C. -M. C.

DECLARATION OF INTERESTS

The authors declare no competing interests.

REFERENCES AND NOTES

(1) Sijbesma, R. P.; Beijer, F. H.; Brunsveld, L.; Folmer, B. J.; Ky Hirschberg, J. H. K.; Lange, R. F. M.; Lowe, J. K. L.; Meijer, E. W. (1997). Reversible polymers formed from self-complementary monomers using quadruple hydrogen bonding. Science *278*, 1601-1604.

(2) Fouquey, C.; Lehn, J.-M.; Levelut, A.-M. (1990). Molecular recognition directed self-assembly of supramolecular liquid crystalline polymers from complementary chiral components. Adv. Mater. *2*, 254-257.

(3) Korevaar, P. A.; George, S. J.; Markvoort, A. J.; Smulders, M. M. J.; Hilbers, P. A. J.; Schenning, A. P. H. J.; De Greef, T. F. A.; Meijer, E. W. (2012). Pathway complexity in supramolecular polymerization. Nature *481*, 492-496.

(4) Ogi, S.; Stepanenko, V.; Thein, J.; Würthner, F. (2016). Impact of alkyl spacer length on aggregation pathways in kinetically controlled supramolecular polymerization. J. Am. Chem. Soc. *138*, 670-678.

(5) Qin, B.; Zhang, S.; Song, Q.; Huang, Z.; Xu, J. -F.; Zhang, X. (2017). Supramolecular interfacial polymerization: a controllable method of fabricating supramolecular polymeric materials. Angew. Chem. Int. Ed. *56*, 7639-7643.

(6) Dong, S.; Zheng, B.; Wang, F.; Huang, F. (2014). Supramolecular polymers constructed from macrocycle-based host-guest molecular recognition motifs. Acc. Chem. Res. *47*, 1982-1994.

(7) Aida, T.; Meijer, E. W.; Stupp, S. I. (2012). Functional supramolecular polymers. Science *335*, 813-817.

(8) Rupar, P. A.; Chabanne, L.; Winnik, M. A.; Manners, I. (2012). Non-centrosymmetric cylindrical micelles by unidirectional growth. Science *337*, 559-562.

(9) Ogi, S.; Sugiyasu, K.; Manna, S.; Samitsu, S.; Takeuchi, M. (2014). Living supramolecular polymerization realized through a biomimetic approach. Nat. Chem. *6*, 188-195.

(10) Kang, J.; Miyajima, D.; Mori, T.; Inoue, Y.; Itoh, Y.; Aida, T. (2015). A rational strategy for the realization of chain-growth supramolecular polymerization. Science *347*, 646-651.

(11) Aliprandi, A.; Mauro, M.; De Cola, L. (2016). Controlling and imaging biomimetic self-assembly. Nat. Chem. *8*, 10-15.

(12) Wagner, W.; Wehner, M.; Stepanenko, V.; Ogi, S.; Würthner, F. (2017). Living supramolecular polymerization of a perylene bisimide dye into fluorescent J-aggregates. Angew. Chem. Int. Ed. *56*, 16008-16012.

(13) Greciano, E. E.; Matarranz, B.; Sánchez, L. (2018). Pathway complexity versus hierarchical self-assembly in *N*-annulated perylenes: structural effects in seeded supramolecular polymerization. Angew. Chem. Int. Ed. *57*, 4697-4701.

(14) Pal, A.; Malakoutikhah, M.; Leonetti, G.; Tezcan, M.; Colomb-Delsuc, M.; Nguyen, V. D.; van der Gucht, J.; Otto, S. (2015). Controlling the structure and length of self-synthesizing supramolecular polymers through nucleated growth and disassembly. Angew. Chem. Int. Ed. *54*, 7852-7856.

(15) Ogi, S.; Matsumoto, K.; Yamaguchi, S. (2018). Seeded polymerization through the interplay of folding and aggregation of an amino-acid-based diamide. Angew. Chem. Int. Ed. *57*, 2339-2343.

(16) Ma, X.; Zhang, Y.; Zhang, Y.; Liu, Y.; Che, Y.; Zhao, J. (2016). Fabrication of chiral-selective nanotubular heterojunctions through living supramolecular polymerization. Angew. Chem. Int. Ed. *55*, 9539-9543.

(17) Jung, S. H.; Bochicchio, D.; Pavan, G. M.; Takeuchi, M.; Sugiyasu, K. (2018). A block supramolecular polymer and its kinetically enhanced stability. J. Am. Chem. Soc. *140*, 10570-10577.

(18) Jin, X.-H.; Price, M. B.; Finnegan, J. R.; Boott, C. E.; Richter, J. M.; Rao, A.; Menke, S. M.; Friend, R. H.; Whittell, G. R.; Manners, I. (2018). Long-range exciton transport in conjugated polymer nanofibers prepared by seeded growth. Science *360*, 897-900.

(19) Wang, X.; Guerin, G.; Wang, H.; Wang, Y.; Manners, I.; Winnik, M. A. (2007). Cylindrical block copolymer micelles and co-micelles of controlled length and architecture. Science *317*, 644-647.

(20) Sampedro, A.; Ramos-Torres, Á.; Schwöppe, C.; Mück-Lichtenfeld, C.; Helmers, I.; Bort, A.; Díaz-Laviada, I.; Fernández, G. (2018). Hierarchical self-assembly of BODIPY dyes as a tool to improve the antitumor activity of capsaicin in prostate cancer. Angew. Chem. Int. Ed. *57*, 17235-17239.

(21) He, F.; Gädt, T.; Manners, I.; Winnik, M. A. (2011). Fluorescent "barcode" multiblock co-micelles via the living self-assembly of di-and triblock copolymers with a crystalline core-forming metalloblock. J. Am. Chem. Soc. *133*, 9095-9103.

(22) Zhang, W.; Jin, W.; Fukushima, T.; Saeki, A.; Seki, S.; Aida, T. (2011). Supramolecular linear heterojunction composed of graphite-like semiconducting nanotubular segments. Science *334*, 340-343.

(23) Liu, Y.; Yu, Y.; Gao, J.; Wang, Z.; Zhang, X. (2010). Water-soluble supramolecular polymerization driven by multiple host-stabilized charge-transfer interactions. Angew. Chem. Int. Ed. *49*, 6576-6579.

(24) Adelizzi, B.; Aloi, A.; Markvoort, A. J.; Ten Eikelder, H. M.; Voets, I. K.; Palmans, A. R. A.; Meijer, E. W. (2018). Supramolecular block copolymers under thermodynamic control. J. Am. Chem. Soc. *140*, 7168-7175.

(25) Qiu, H.; Gao, Y.; Boott, C. E.; Gould, O. E.; Harniman, R. L.; Miles, M. J.; Webb, S. E.; Winnik, M. A.; Manners, I. (2016). Uniform patchy and hollow rectangular platelet micelles from crystallizable polymer blends. Science *352*, 697-701.

(26) Adelizzi, B.; Van Zee, N. J.; de Windt, L. N. J.; Palmans, A. R. A.; Meijer, E. W. (2019). The future of supramolecular copolymers unveiled by reflecting on covalent copolymerization. J. Am. Chem. Soc. *141*, 6110−6121.

(27) Hudson, Z. M.; Lunn, D. J.; Winnik, M. A.; Manners, I. (2014). Colour-tunable fluorescent multiblock micelles. Nature communications *5*, 3372.

(28) Wagner, W.; Wehner, M.; Stepanenko, V.; Würthner, F. (2019). Supramolecular block copolymers by seeded living polymerization of perylene bisimides. J. Am. Chem. Soc. *141*, 12044-12054.

(29) Liu, Q.; Xie, M.; Chang, X.; Cao, S.; Zou, C.; Fu, W.-F.; Che, C.-M.; Chen, Y.; Lu, W. (2018). Tunable multicolor phosphorescence of crystalline polymeric complex salts with metallophilic backbones. Angew. Chem. Int. Ed. *57*, 6279-6283.

(30) Wan, Q.; To, W.-P.; Yang, C.; Che, C.-M. (2018). The metal-metal-to-ligand charge transfer excited state and supramolecular polymerization of luminescent pincer Pd^{II}-isocyanide complexes. Angew. Chem. Int. Ed. *57*, 3089-3093.

(31) Roundhill, D. M.; Gray, H. B.; Che, C.-M. (1989). Pyrophosphito-bridged diplatinum chemistry. Acc. Chem. Res. *22*, 55-61.

(32) Ly, K. T.; Chen-Cheng, R.-W.; Lin, H.-W.; Shiau, Y.-J.; Liu, S.-H.; Chou, P.-T.; Tsao, C.-S.; Huang, Y.-C.; Chi, Y. (2017). Near-infrared organic light-emitting diodes with very high external quantum efficiency and radiance. Nat. Photonics *11*, 63-68.

(33) Li, K.; Tong, G. S. M.; Wan, Q.; Cheng, G.; Tong, W.-Y.; Ang, W.-H.; Kwong, W.-L.; Che, C.-M. (2016). Highly phosphorescent platinum(II) emitters: photophysics, materials and biological applications. Chem. Sci. *7*, 1653-1673.

(34) Wong, K. M.-C.; Yam, V. W.-W. (2011). Self-assembly of luminescent alkynylplatinum(II) terpyridyl complexes: modulation of photophysical properties through aggregation behavior. Acc. Chem. Res. *44*, 424-434.

(35) Ma, B.; Li, J.; Djurovich, P. I.; Yousufuddin, M.; Bau, R.; Thompson, M. E. (2005). Synthetic control of Pt···Pt separation and photophysics of binuclear platinum complexes. J. Am. Chem. Soc., *127*, 28-29.

(36) Gao, Z.; Han, Y.; Gao, Z.; Wang, F. (2018). Multicomponent assembled systems based on platinum (II) terpyridine complexes. Acc. Chem. Res. *51*, 2719-2729.

(37) Bercaw, J. E.; Durrell, A. C.; Gray, H. B.; Green, J. C.; Hazari, N.; Labinger, J. A.; Winkler, J. R. (2010). Electronic structures of Pd^{II} dimers. Inorg. Chem. *49*, 1801-1810.

(38) Chow, P.-K.; To, W.-P.; Low, K.-H.; Che, C.-M. (2014). Luminescent palladium(II) complexes with π-extended cyclometalated [R-C^N^N-R'] and pentafluorophenylacetylide ligands: spectroscopic, photophysical, and photochemical properties. Chem. -Asian J. *9*, 534-545.

(39) Lai, S.-W.; Cheung, T.-C.; Chan, M. C.; Cheung, K.-K.; Peng, S.-M.; Che, C.-M. (2000). Luminescent mononuclear and binuclear cyclometalated palladium(II) complexes of 6-phenyl-2,2'-bipyridines: spectroscopic and structural comparisons with platinum(II) analogues. Inorg. Chem. *39*, 255-262.

(40) Chow, P.-K.; Ma, C.; To, W.-P.; Tong, G. S. M.; Lai, S. L.; Kui, S. C.; Kwok, W. M.; Che, C.-M. (2013). Strongly phosphorescent palladium(II) complexes of tetradentate ligands with mixed oxygen, carbon, and nitrogen donor atoms: photophysics, photochemistry, and applications. Angew. Chem. Int. Ed. *52*, 11775-11779.

(41) Fleetham, T.; Ji, Y.; Huang, L.; Fleetham, T. S.; Li, J. (2017). Efficient and stable single-doped white OLEDs using a palladium-based phosphorescent excimer. Chem. Sci. *8*, 7983-7990.

(42) Liu, L.; Wang, X.; Hussain, F.; Zeng, C.; Wang, B.; Li, Z.; Kozin, I.; Wang, S. (2019). Multi-responsive tetradentate phosphorescent metal complexes as highly sensitive and robust luminescent oxygen sensors: Pd(II) versus Pt(II) and 1,2,3-triazolyl versus 1,2,4-triazolyl. ACS applied materials & interfaces. *11*, 12666-12674.

(43) Coelho, J. P.; Matern, J.; Albuquerque, R. Q.; Fernández, G. (2019). Mechanistic insights into statistical co-assembly of metal complexes. Chem. Eur. J. *25*, 8960-8964.

(44) Chen, Y.; Lu, W.; Che, C.-M. (2012). Luminescent pincer-type cyclometalated platinum(II) complexes with auxiliary isocyanide ligands: phase-transfer preparation, solvatomorphism, and self-aggregation. Organometallics *32*, 350-353.

(45) Lai, S.-W.; Lam, H.-W.; Lu, W.; Cheung, K.-K.; Che, C.-M. (2002). Observation of low-energy metal-metal-to-ligand charge transfer absorption and emission: electronic spectroscopy of cyclometalated platinum(II) complexes with isocyanide ligands. Organometallics *21*, 226-234.

(46) Yuen, M.-Y.; Roy, V. A. L.; Lu, W.; Kui, S. C. F.; Tong, G. S. M.; So, M.-H.; Chui, S. S.-Y.; Muccini, M.; Ning, J. Q.; Xu, S. J.; Che, C.-M. (2008). Semiconducting and electroluminescent nanowires self-assembled from organoplatinum(II) complexes. Angew. Chem. Int. Ed. *47*, 9895-9899.

(47) De Greef, T. F. A.; Smulders, M. M. J.; Wolffs, M.; Schenning, A. P. H. J.; Sijbesma, R. P.; Meijer, E. W. (2009). Supramolecular polymerization. Chem. Rev. *109*, 5687-5754.

(48) Oosawa, F.; Kasai, M. (1962). A theory of linear and helical aggregations of macromolecules. J. Mol. Biol. *4*, 10-21.

(49) Wan, Q.; Xiao, X.-S.; To, W.-P.; Lu, W.; Chen, Y.; Low, K.-H.; Che, C.-M. (2018). Counteranion and solvent mediated chirality transfer in the supramolecular polymerization of luminescent platinum(II) complexes. Angew. Chem. Int. Ed. *57*, 17189-17193.

(50) Smulders, M. M. J. S. ; Nieuwenhuizen, M. M. L.; de Greef, T. F. A.; van der Schoot, P.; Schenning, A. P. H. J.; Meijer, E. W. (2010). How to distinguish isodesmic from cooperative supramolecular polymerisation. Chem. Eur. J. *16*, 362-367.

(51) Tanase, T.; Tanaka, M.; Hamada, M.; Morita, Y.; Nakamae, K.; Ura, Y.; Nakajima, T. (2019). Alloyed tetranuclear metal chains of $Pd_{4-n}Pt_n$ (n = 0-3) scaffolded by a new linear tetraphosphine containing a PNP bridge. Chem. Eur. J. *25*, 8219-8224.

(52) Hudson, Z. M.; Boott, C. E.; Robinson, M. E.; Rupar, P. A.; Winnik, M. A.; Manners, I. (2014). Tailored hierarchical micelle architectures using living crystallization-driven self-assembly in two dimensions. Nat. Chem. *6*, 893-898.

(53) Fukui, T.; Kawai, S.; Fujinuma, S.; Matsushita, Y.; Yasuda, T.; Sakurai, T.; Seki, S.; Takeuchi, M.; Sugiyasu, K. (2017). Control over differentiation of a metastable supramolecular assembly in one and two dimensions. Nat. Chem. *9*, 493-499.

(54) Wan, Q.; Xia, J.; Lu, W.; Yang, J.; Che, C.-M. (2019). Kinetically controlled self-assembly of phosphorescent Au^{III} aggregates and ligand-to-metal-metal charge transfer excited state: a combined spectroscopic and DFT/TDDFT study. J. Am. Chem. Soc. *141*, 11572-11582.

(55) Zhao, D.; Moore, J. S. (2003). Nucleation-elongation: a mechanism for cooperative supramolecular polymerization. Organic & biomolecular chemistry *1*, 3471-3491.

(56) Oosawa, F.; Asakura, S. Thermodynamics of the Polymerization of Protein; Academic Press, 1975, 3553.

(57) McGlynn, S.; Azumi, T.; Kasha, M. (1964). External heavy-atom spin-orbital coupling effect. V. Absorption studies of triplet states. J. Chem. Phys. *40*, 507-515.

(58) Bolton, O.; Lee, K.; Kim, H.-J.; Lin, K. Y.; Kim, J. (2011). Activating efficient phosphorescence from purely organic materials by crystal design. Nat. Chem. *3*, 205-210.

(59) Kasha, M. (1952). Collisional perturbation of spin-orbital coupling and the mechanism of fluorescence quenching. a visual demonstration of the perturbation. J. Chem. Phys. *20*, 71-74.

(60) Carretero, A. S.; Castillo, A. S.; Gutiérrez, A. F. (2005). A review of heavy-atom-induced room-temperature phosphorescence: A straightforward phosphorimetric method. Crit. Rev. Anal. Chem. *35*, 3-14.

(61) Murakami, M.; Ohkubo, K.; Nanjo, T.; Souma, K.; Suzuki, N.; Fukuzumi, S. (2010). Photoinduced electron transfer in photorobust coumarins linked with electron donors affording long lifetimes of triplet charge-separated states. ChemPhysChem *11*, 2594-2605.

(62) Pellow, R.; Vala, M. (1989). The external heavy atom effect: theory of spin-orbit coupling of alkali and noble metals in rare gas matrices. J. Chem. Phys. *90*, 5612-5621.